European Polymer Journal 81 (2016) 12–23

Contents lists available at ScienceDirect

European Polymer Journal

journal homepage: www.elsevier.com/locate/europolj

High-strength semi-crystalline hydrogels with self-healing and shape memory functions

Burcu Kurt, Umit Gulyuz, Damla D. Demir, Oguz Okay *

Istanbul Technical University, Department of Chemistry, 34469 Istanbul, Turkey

ARTICLE INFO

Article history:
Received 12 March 2016
Received in revised form 16 May 2016
Accepted 19 May 2016
Available online 20 May 2016

Keywords:
Supramolecular hydrogels
Crystallinity
Hydrophobic associations
Shape memory
Self-healing
Mechanical properties

ABSTRACT

We present a non-covalent approach and bulk photopolymerization method of hydrophilic and hydrophobic monomers to generate high-strength self-healing hydrogels with shape-memory effect. The hydrogels consist of linear poly(N,N-dimethylacrylamide) (PDMA) or polyacrylic acid (PAAc) chains containing (meth)acrylate units with long alkyl side chains. The existence of crystalline domains and hydrophobic associations formed by side alkyl chains produces hybrid-crosslinked PDMA and PAAc hydrogels with particularly high fracture energy of 20 ± 1 kJ m^{-2} and Young's modulus up to 308 ± 16 MPa. The mechanical properties of the hydrogels could be tailored by varying the degree of crystallinity. By choosing suitable comonomer pairs and compositions, one may vary the degree of crystallinity between 3 and 33%, which leads to two orders of magnitude change in the modulus, elongation at break, and toughness. The hydrogels undergo up to 1000 fold change in their elastic moduli by changing the temperature between below and above the melting temperature of the crystalline regions. They also exhibit self-healing and shape memory functions triggered by heating above the melting temperature. Healed hydrogels sustain up to 138 ± 10 MPa compressive stresses, which are around 87% of the compressive stress of the virgin gel samples.

1. Introduction

Hydrogels are crosslinked hydrophilic polymers capable of retaining water without dissolving. Softness, smartness, elasticity, similarity to biological tissues, and excellent permeability for transport of nutrient and metabolites make hydrogels unique materials [1,2]. One of the obvious limitations of conventional synthetic hydrogels compared to many biological gel composites (such as cartilage and cornea) is their poor mechanical properties, with fracture energies around 10 J m^{-2} and a mechanical strength of below MPa level [3–5]. This mechanical weakness is mainly due to the lack of an effective energy dissipation mechanism in the covalently crosslinked gel network [3,5–7]. Several techniques have been developed in the past decade to increase the extent of energy dissipation in the gel network and hence to produce tough hydrogels [8]. Fig. 1 summarizes some recent achievements in the gel science where the Young's modulus E and the tensile fracture stress σ_f of stress-bearing, new generation hydrogels are plotted against their fracture energies G [9–20].

A milestone in the development of such soft materials is the double-network (DN) hydrogels exhibiting a high mechanical strength up to 10 MPa [9–11]. DN concept bases on the co-existence of interlinked and interpenetrated brittle and ductile chemically crosslinked polymer networks. Under large strain, the highly crosslinked brittle network internally ruptures

* Corresponding author.
E-mail address: okayo@itu.edu.tr (O. Okay).

http://dx.doi.org/10.1016/j.eurpolymj.2016.05.019
0014-3057/

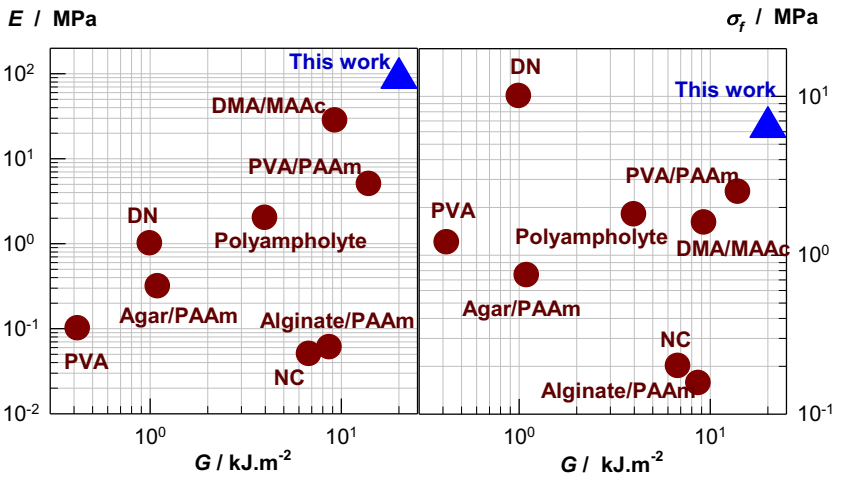

Fig. 1. Young's modulus E, tensile fracture stress σ_f, and fracture energy G of new generation hydrogels [9–20]. The abbreviations are explained in the text. The maximum reported values in the literature are shown. The data of the present work are from DMA/C18A hydrogel with 30 mol% hydrophobe.

by dissipating energy while the slightly crosslinked ductile network keeps the gel surface together. The shortcoming of this technique is the permanent damage of the first brittle network even under low strain conditions, leading to an irreversible deformation of DN hydrogels. To address this problem, hybrid DNs have been synthesized consisting of interpenetrated chemically and physically crosslinked network components such as agar/polyacrylamide (Agar/PAAm) [12], polyvinyl alcohol/PAAm (PVA/PAAm) [13], and alginate/PAAm hydrogels [14]. Although hybrid DNs exhibit reversible mechanical cycles and higher fracture energies as compared to the classical DNs, their fracture stresses are relatively low due to the presence of non-covalent bonds (Fig. 1). PVA hydrogels obtained by directional freezing-thawing technique exhibit tensile strengths up to 1.2 MPa [15]. Nanocomposite (NC) hydrogels prepared by in situ polymerization of hydrophilic monomers in aqueous solutions of Laponite, a hectorite synthetic clay, exhibit high fracture energies (up to 6.8 kJ m^{-2}) and elongation to break (>1500%) [16–18]. Another class of high-strength hydrogels is the polyampholytes consisting of strong and weak physical bonds due to the inhomogeneous distribution of electrostatic interactions [19]. Recent work by Hu et al. has demonstrated that the copolymerization of N,N-dimethylacrylamide (DMA) and methacrylic acid (MAAc) in aqueous solutions produces hydrogels with the highest Young's modulus E (28 MPa) so far reported (Fig. 1) [20]. Formation of polymer-rich aggregates via H-bonding stabilized by the hydrophobic interactions due to the presence of the α-methyl groups of MAAc units seems to be responsible for the good mechanical performance of DMA/MAAc hydrogels (Fig. 1). Several strategies have also been presented in the past decade to generate supramolecular hydrogels with self-healing properties [21–30]. Moreover, dual-functional hydrogel systems combining self-healing with shape memory effect have drawn attention in recent years [31–33].

High-strength hydrogels reported before generally use in situ polymerization which is lengthy and complicated. For instance, DN hydrogels are prepared by swelling a highly crosslinked first-network hydrogel in a solution of a second monomer and then polymerizing the second monomer in situ to form a loosely crosslinked second-network. Moreover, most of the hydrogels have no shape-memory properties and lack the ability to heal themselves when damaged. On the whole, alternate simple one-pot synthesis methods are needed to design high-strength hydrogels that offer complete self-healing and shape-memory abilities. Here, we introduce a simple non-covalent approach and bulk photopolymerization method of hydrophilic and hydrophobic comonomers owing to the advantages for easy preparation and the potential self-healing and shape-memory capabilities of the products. We use hydrophobic interactions to generate a 3D network of hydrophilic polymer chains interconnected by alkyl side chain crystals and hydrophobic associations. The hydrogels we described here consist of linear poly(N,N-dimethylacrylamide) (PDMA) or polyacrylic acid (PAAc) chains containing 20–50 mol% (meth)acrylate units with long alkyl side chains. Gelation under bulk conditions as well as formation of alkyl crystals and hydrophobic associations acting as strong and weak crosslinks, respectively, produce PDMA and PAAc hydrogels with particularly high fracture energy of 20 ± 1 kJ m^{-2} and Young's modulus up to 308 ± 16 MPa (Fig. 1). The hydrogels exhibit self-healing and shape memory functions triggered by heating above the melting temperature of their crystalline domains.

2. Experimental

2.1. Materials

N,N-dimethylacrylamide (DMA, Aldrich) and acrylic acid (AAc, Merck) were freed from the inhibitor by passing through an inhibitor removal column purchased from the Aldrich Chemical Co. Commercially available stearyl methacrylate (C17.3M, Aldrich) consists of 65% *n*-octadecyl methacrylate and 35% *n*-hexadecyl methacrylate. *n*-octadecyl acrylate (C18A, Sigma) and Irgacure 2959 (Aldrich) were used as received.

2.2. Hydrogel preparation and gel fraction measurements

The hydrogels were prepared by bulk copolymerization of DMA or AAc with the hydrophobic monomer C17.3M or C18A in the presence of Irgacure 2959 as the photoinitiator at a concentration of 0.1 wt% (with respect to the monomers). The hydrophobe content of the comonomer feed was varied between 20 and 50 mol%. The comonomer pairs DMA/C17.3M, DMA/C18A, and AAc/C18A were first mixed and thoroughly stirred at 45 °C. After addition of the initiator Irgacure 2959, the monomer mixtures containing the initiator were transferred into several pipettes of 4.7 mm in diameter as well as between two glass plates (5 × 5 or 20 × 2 cm) separated by a 0.5 mm silicone spacer. The polymerization was conducted at 23 ± 2 °C for 1 day under UV lamp at a wavelength of 360 nm. After polymerization, the copolymer samples were immersed in a large amount of water for several days by replacing water every day to extract any soluble species. The water temperature was 70 °C and 23 ± 2 °C for the first and following days, respectively. The initial high-temperature immersion period above the melting temperature of the crystalline domains of the hydrogels is to provide that the network chains assume their relaxed state so that a complete shape-memory effect could be observed. After equilibrium swelling in water, the relative mass m_{rel} of the hydrogels at 23 ± 2 °C with respect to the gel mass after preparation state was calculated as $m_{rel} = m/m_0$, where m_0 and m are the initial and swollen mass of the gel samples. Then, the gel samples were taken out of water and freeze-dried. The water content of the hydrogels was calculated as $H_2O\% = 10^2\ (m - m_{dry})/m$, where m_{dry} is the dried mass of the gel sample. The gel fraction W_g, that is, the conversion of monomers to the water-insoluble polymer was calculated from the masses of dry polymer network and from the comonomer feed.

2.3. Rheological experiments

Rheological measurements were performed on Gemini 150 Rheometer system, Bohlin Instruments, equipped with a Peltier device for temperature control. Hydrogel samples equilibrium swollen in water were subjected to dynamic experiments between the parallel plates of the rheometer. The upper plate (diameter 20 mm) was set at a distance of 650–1300 μm, depending on the swelling degree of the hydrogels. During all measurements, a solvent trap was used to minimize the evaporation. Further, the outside of the upper plate was covered with a thin layer of low-viscosity silicone oil to prevent evaporation of solvent. Viscoelastic behavior of the hydrogels depending on temperature was measured during heating-cooling cycles between 5 and 80 °C at a fixed rate of 1 °C/min. An angular frequency of $\omega = 6.28$ rad/s and a deformation amplitude $\gamma_0 = 0.001$ (0.1%) were selected to ensure that the oscillatory deformation is within the linear regime. The changes in the dynamic moduli of gels were monitored during the course of the cycle as a function of temperature. The samples were also subjected to frequency sweep tests at $\gamma_0 = 0.001$.

2.4. DSC measurements

DSC measurements were conducted on a Perkin Elmer Diamond DSC under a nitrogen atmosphere. The gel samples equilibrium swollen in water were cut into small specimens of about 10 mg weight and sealed in aluminum pans. Then, they were scanned between 5 and 80 °C with a heating and cooling rate of 5 °C/min. From the DSC curves, enthalpy changes during melting, ΔH_m, were calculated from the peak areas. The degree of crystallinity, f_{cry}, that is, the fraction of polymer units in crystalline domains, was estimated by $f_{cry} = x_{HM}\Delta H_m/\Delta H_m^o$, where x_{HM} is the mole fraction of the hydrophobic monomer in the comonomer feed and ΔH_m^o is the melting enthalpy of crystalline C17.3M and C18A units. ΔH_m^o was taken as 71.2 kJ mol^{-1} from previous works on the melting behavior of long *n*-alkyl chains exhibiting a hexagonal crystal structure [34–37]. The fraction $f_{non\text{-}cry}$ of hydrophobic monomer units in non-crystalline domains was estimated by $f_{non-cry} = x_{HM} - f_{cry}$.

2.5. X-ray diffraction (XRD) measurements

XRD pattern were collected on a PANalytical X'Pert Pro diffractometer system equipped with Pixel-Array detector at a fixed divergence optic for incident beam in a Bragg-Brentano geometry, and a Cu Kα source with nickel filter ($\lambda = 0.15406$ nm). Measurements were carried out at room temperature with sample and empty substrate for background subtraction between 10° and 40° 2θ range, with a scan rate of 0.5°/min.

2.6. Mechanical tests

Uniaxial compression and elongation measurements were performed on swollen hydrogel samples on Zwick Roell and Devotrans test machines with 500 N and 10 kN load cells. All the tests were conducted in a thermostated room at 23 ± 2 °C. Load and displacement data were collected during the experiments. The Young's modulus *E* was calculated from the slope of stress–strain curves between 5–15% and 1–3% deformations for compression and elongation tests, respectively. For uniaxial compression measurements, cylindrical hydrogel samples of 5 mm in diameter and 5 ± 1 mm in length were compressed at strain rates 3.8×10^{-3} and 3.8×10^{-2} s^{-1}. Before the test, an initial compressive contact to 0.01 ± 0.002 N was applied to ensure a complete contact between the gel and the plates. The stress was presented by its nominal σ_{nom} or true values σ_{true} ($=\lambda\sigma_{nom}$), which are the forces per cross-sectional area of the undeformed and deformed gel specimen

respectively, while the compressive strain is given by λ, the deformation ratio (deformed length/initial length). The strain is also given by ε, the change in the sample length relative to its initial length, i.e., $\varepsilon = 1 - \lambda$ or $\varepsilon = \lambda - 1$ for compression and elongation tests, respectively. We have to mention that the gel samples did not break even at a strain of about 100% compression, and therefore, the nominal stress σ_{nom} increased continuously with increasing strain. However, the corresponding σ_{true}–λ plots pass through maxima indicating the onset of failure in the gel specimen. Therefore, the nominal fracture stress σ_f and the compression ratio λ_f at failure were calculated from the maxima in σ_{true}–λ plots (Fig. S1). The energy to break (toughness) W was calculated from the area below the nominal stress-strain curves up to the fracture point. The cyclic compression tests were conducted at a constant strain rate of $3.8 \times 10^{-3}\ s^{-1}$ to a maximum compression ratio, followed by retraction to zero force and a waiting time of 5 min at 70 °C in water, until the next cycle of compression. Uniaxial elongation measurements were performed on dumbbell-shaped hydrogel samples with the standard ISO-37 type 2 (ISO 527-2) under following conditions: Strain rate = between 7.8×10^{-2} and $4 \times 10^{-3}\ s^{-1}$; sample length between jaws = 43 ± 2 mm. Cyclic elongation tests were conducted as the compression cycles except that the strain rate was set to $3.8 \times 10^{-2}\ s^{-1}$. We have to note that the duration of the mechanical tests was less than 18 min during which no change could be observed in the mass of the gel samples. The tearing tests were performed on hydrogel samples that were cut into the standard JIS-K6252 1/2 sizes (length = 50 mm, width = 7.5 mm, thickness = 0.75–1.25 mm, length of the initial notch = 20 mm). The two arms of the gel sample were clamped, and then the upper arm was pulled upward at a constant rate of 100 mm/min while the tearing force F was recorded. The fracture (tearing) energy G was calculated at a constant tearing force F using the relation G = 2F/w, where w is the thickness of the sample [10,19].

2.7. Self-healing behavior

The virgin hydrogel samples after equilibrium swelling in water were cut in the middle, and then the two halves were merged together within a plastic syringe (of the same diameter as the gel sample) at 80 °C by slightly pressing the piston plunger. To quantify the healing efficiency, uniaxial compression tests were performed on virgin and healed cylindrical hydrogel samples.

2.8. Shape memory behavior

Bending tests were utilized to examine the shape memory properties of the hydrogels. Hydrogel samples equilibrium swollen in water were folded at 70 °C and then cooled down to 20° to fix the bent shape. Then, bent hydrogel sample in a water bath was stepwise heated from 20 to 70 °C at 1 °C steps. At each temperature T, the final angle θ_T was recorded after it has been steady. The measurements of θ_T were conducted using an image analyzing system consisting of a microscope (XSZ single Zoom microscope), a CDD digital camera (TK 1381 EG) and a PC with the data analyzing system Image-Pro Plus. The shape recovery ratio R was calculated as $R = \theta_T/180$.

3. Results and discussion

We have prepared the hydrogels by bulk polymerization of the hydrophilic monomer DMA or AAc without the addition of a multifunctional crosslinker. Instead, a hydrophobic monomer having a long alkyl side chain was added to generate physical crosslinks between PDMA and PAAc chains. Stearyl methacrylate (C17.3M) is one of the hydrophobes used in this study, which is a mixture of *n*-octadecyl methacrylate and *n*-hexadecylacrylate with an average alkyl chain length of 17.3 carbon atoms. The other hydrophobe is *n*-octadecyl acrylate (C18A) with a side chain length of 18 carbons. Because both DMA and AAc are liquid under ambient condition and miscible with the hydrophobes C17.3M and C18A, no solvent is needed for the preparation of the pregel solutions. Three different combinations of the comonomer pairs with hydrophobe contents between 20 and 50 mol% were prepared, namely DMA/C17.3M, DMA/C18A, and AAc/C18A (Table 1). The polymerization reactions initiated using Irgacure 2959 initiator under UV light resulted in copolymers with a gel fraction of unity, indicating that all the monomers in the feed are incorporated into the polymer network (Fig. S2). The copolymers were insoluble in organic solvents such as ethanol, THF, DMSO, and DMF. The copolymer hydrogels in equilibrium with water contained 7–56% water, which decreased with increasing hydrophobe content (Table 1, Fig. S2). Moreover, except for the hydrophobe content of 50 mol%, the water content also decreased by replacing the hydrophobic monomer C17.3M with C18A.

Fig. 2A shows XRD patterns of the swollen hydrogels between 10 and 40° 2θ range. They all exhibit a peak at $2\theta = 21.6°$ corresponding to an interlamellar *d*-spacing of 0.41 nm. This *d*-spacing reveals hexagonal packing of side C17.3 and C18 chains within the swollen gel network [38]. For the hydrogels with 50% hydrophobe (red curves in the figures), a sharp diffraction peak of crystallized alkyl side chains is observed while, with decreasing hydrophobe content, the peak becomes broader indicating that a decreasing fraction of alkyl chains is incorporated into the crystalline domains. DSC traces of water-swollen hydrogel samples indeed reveal melting and crystallization transitions by changing the temperature (Fig. S3). Fig. 2B shows the melting T_m, and crystallization temperatures T_{cry} together with the degree of crystallinity f_{cry} of the hydrogels plotted against the hydrophobe content. General trend is that, both the transition temperatures and the degree of crystallinity increase with increasing hydrophobe level, or by replacing C17.3M hydrophobe with C18A (curves 1 vs 2 in Fig. 2b). Higher thermal stability of the crystalline domains formed from C18A monomer is attributed to the uniform length of its side alkyl

Table 1
Characteristic data and tensile properties of the hydrogels.

Code	x_{HM}[a]	H_2O %	T_m °C	T_{cry} °C	f_{cry}[b] %	$f_{non\text{-}cry}$[c] %	E[d] MPa	σ_f[e] MPa	ε_f[f] %	W[g] MJ m^{-3}	G[h] kJ m^{-2}
DMA/C17.3M	0.20	56	38	26	3.4	16.6	4 (1)	1.5 (0.1)	440 (50)	5 (1)	3.6 (0.2)
	0.30	36	37	26	7.8	22.2	9 (1)	2.3 (0.2)	390 (40)	6 (1)	9 (1)
	0.50	7	36	23	13	37	28 (9)	2.8 (0.5)	300 (10)	6 (1)	16 (1)
DMA/C18A	0.20	47	40	35	3	17	6 (1)	2.1 (0.3)	443 (96)	8 (3)	11 (2)
	0.30	29	49	39	10	20	89 (20)	6.4 (0.2)	13 (3)	1.1 (0.2)	20 (1)
	0.50	11	51	40	28	22	159 (17)	6.7 (0.8)	5 (1)	0.2 (0)	Brittle
AAc/C18A	0.20	35	48	45	10	10	24 (4)	3.3 (0.6)	91 (25)	3 (1)	18 (1)
	0.30	27	52	44	19	11	79 (11)	3.5 (0.4)	6 (3)	0.1 (0)	Brittle
	0.50	11	56	46	33	17	308 (16)	5.1 (0.1)	2 (1)	0.05 (0.01)	Brittle

Strain rate for the tensile tests is 3.8×10^{-2} s^{-1} while for the tearing tests, it is 100 mm min^{-1} (4.2×10^{-2} s^{-1}) (standard deviations in parentheses while for H_2O%, f_{cry}, T_m, and T_{cry}, they are less than 8%).

[a] Mole fraction of the hydrophobic monomer in the feed.
[b] Degree of crystallinity.
[c] Fraction of the hydrophobic monomer units in non-crystalline domains.
[d] Young's modulus.
[e] Tensile fracture stress.
[f] Strain at break.
[g] Energy to break (toughness).
[h] Fracture (tearing) energy.

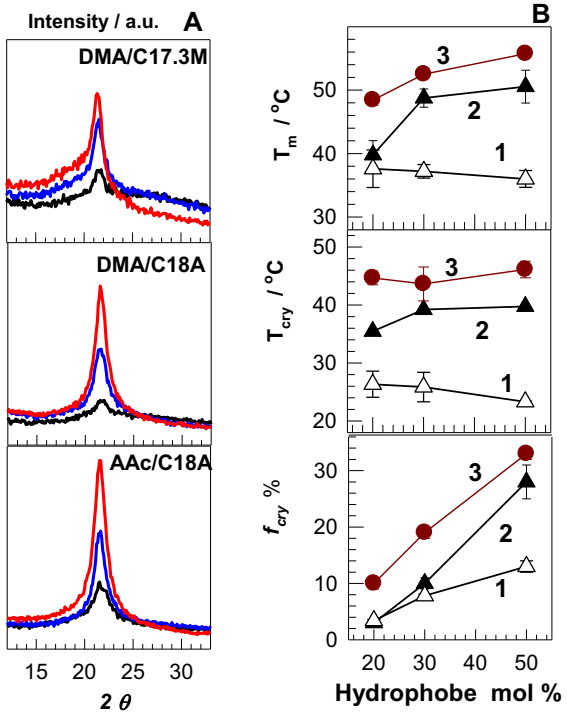

Fig. 2. (A) XRD patterns of the hydrogels with 20 (black curves), 30 (blue curves), and 50 mol% hydrophobe (red curves). (B) T_m, T_{cry}, and the degree of crystallinity f_{cry} of DMA/C17.3M (1), DMA/C18A (2), and AAc/C18A hydrogels (3) plotted against their hydrophobe content. (For interpretation of the references to colour in this figure legend, the reader is referred to the web version of this article.)

chain as well as to the flexibility of acrylate backbones as compared to methacrylate ones. Moreover, PAAc backbone produces a higher transition temperature and degree of crystallinity as compared PDMA backbone (curves 3 vs 2 in Fig. 2b), which we attribute to the cooperative hydrogen bonding between the carboxyl groups of AAc units stabilizing the alkyl crystals [39]. The results in Fig. 2 thus reveal that the stability of crystalline domains in the hydrogels increases in the following order: DMA/C17.3M < DMA/C18A < AAc/C18A.

The melting and re-crystallization of crystalline domains depending on a change in temperature resulted in drastic changes in the viscoelastic behavior of the hydrogels (Fig. S4). This is illustrated in Fig. 3A where the variations of the elastic modulus G' (filled symbols), the viscous modulus G'' (open symbols), and the loss factor tan δ (=G''/G', lines) of hydrogel

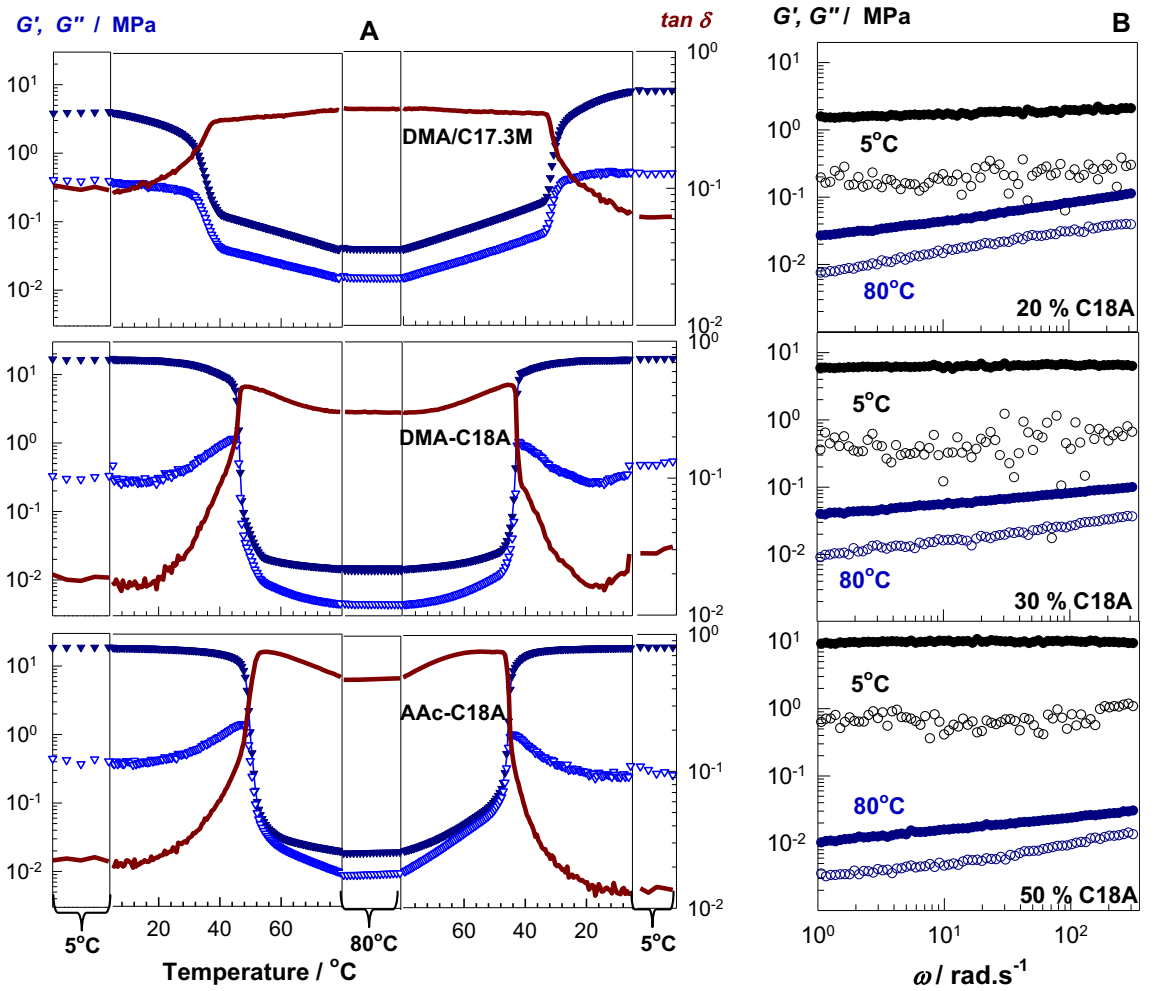

Fig. 3. (A) G' (filled symbols), G'' (open symbols) and tan δ (lines) of the hydrogels during the heating - cooling cycle between 80 and 5 °C. The type of the hydrogels indicated. Note that G' is always larger than G'' over the whole temperature range. Hydrophobe content = 50 mol%. ω = 6.28 rad s^{-1}. γ_o = 0.001. (B) G' (filled symbols) and G'' (open symbols) of DMA/C18A hydrogels with 20, 30, and 50 mol% hydrophobe at 5 and 80 °C shown as a function of the frequency ω. γ_o = 0.001.

samples with 50 mol% hydrophobe are shown during the course of the heating and cooling periods between below and above the transition temperatures. The elastic modulus G' is between 4 and 19 MPa at 5 °C while, upon heating above T_m, it 100–1000 fold decreases and becomes 14–39 kPa at 80 °C. DMA/C17.3M hydrogel exhibits the highest loss factor tan δ among others indicating larger energy dissipation. As seen in Table 1, the degree of crystallinity is smaller while the fraction $f_{non\text{-}cry}$ of non-crystalline alkyl side chains is higher in DMA/C17.3M hydrogel as compared to the other hydrogels. The existence of a larger number of non-crystalline alkyl side chains in this hydrogel seems to be responsible for the dissipation of a large amount of energy under deformation.

The hydrogels at below and above T_m were subjected to frequency-sweep tests at a strain amplitude γ_o = 0.001 over the frequency (ω) range 1–400 rad s^{-1}. The results of the measurements are shown in Fig. 3B for DMA/C18A hydrogels at various C18A contents. Note that some scatter in G'' data at 5 °C is due to the sensitivity limit of the rheometer in the determination of the phase angle δ. The elastic modulus G' is always higher than the viscous modulus G'' indicating that the hydrogels at both above and below T_m remain in the gel state over the whole range of frequency. Below T_m (at 5 °C), G' increases only slightly with frequency with an exponent varying from 0.07 (20 mol% C18A) to 0.02 (50 mol% C18A) while the loss factor tan δ remains at around 0.10. The quantity tan δ representing the ratio of dissipated energy to stored energy during one deformation cycle is usually in the range of 10^{-2} to 10^{-3} for chemically crosslinked hydrogels [40]. Thus, although the hydrogels in the semi-crystalline state exhibit an elastic modulus at the MPa level, significant viscoelastic dissipation occurs during their deformation. Above T_m (at 80 °C), the modulus G' exhibits a much stronger frequency-dependence with an exponent between 0.15 and 0.23 while tan δ increases above 0.1 corresponding to weak gel behavior. Similar results were also observed for DMA/C17.3M and AAc/C18A hydrogels (Fig. S5). The results thus indicate the dynamic nature of the hydrogels which we attribute to the hydrophobic units in non-crystalline domains forming hydrophobic associations.

Mechanical properties of water-swollen hydrogels were investigated by uniaxial compression and elongation tests. Fig. 4A represents typical stress-strain data of the hydrogels at 23 ± 2 °C and at a strain rate of 3.8×10^{-2} s^{-1}, as the dependence of the nominal stress σ_{nom} on the deformation ratio λ (deformed length/initial length). In compression tests ($\lambda < 1$), the hydrogels sustain up to 90% compressions and 40–100 MPa compressive stresses (Fig. S6). The results of tensile tests are compiled in Table 1 and Fig. 4B, where the Young's modulus E, fracture stress σ_f, fracture strain ε_f, and energy to break (toughness) W are plotted against the degree of crystallinity f_{cry}. It is seen that all the mechanical data of the hydrogels almost collapse into a single curve when they are plotted against f_{cry} as the independent parameter. Similar results were also obtained for the compressive test results (Fig. S6).

By choosing suitable comonomer pairs and compositions, one may vary f_{cry} between 3 and 33%, which leads to two orders of magnitude change in the modulus, elongation at break, and toughness. For instance, the modulus E increases with increasing f_{cry} and becomes 308 ± 16 MPa at f_{cry} = 33%, which is the highest modulus reported so far for high-strength hydrogels. It needs to be mentioned that the high strength hydrogels prepared in the past decade have different water contents making direct comparisons of the modulus difficult. To make a reasonable comparison, one has to calculate the elastically effective crosslink density ν_e of the networks from the Young's modulus E. For an affine network of Gaussian chains, the modulus E is related to the crosslink density ν_e of the network by [41,42]:

$$E = 3\nu_e RT \nu_2^{1/3} \nu_2^{o2/3} \quad (1)$$

where ν_2^o and ν_2 are the volume fractions of polymer at the state of preparation and at the measurement state, respectively, R is the gas constant and T is the absolute temperature. ν_2^o equals to unity for the present hydrogels and ν_2 = 0.89 for the AAc/C18A hydrogel at f_{cry} = 33% (Table 1). Thus, E = 308 ± 16 MPa corresponds to ν_e = 43 ± 2 kmol m^{-3}. Since the highest modulus of the hydrogel reported before was 28 ± 2 MPa [20], similar calculations using $\nu_2^o = \nu_2$ = 0.33 lead to ν_e = 11 ± 1 kmol m^{-3} which is about 4-fold lower than that of the present hydrogel.

Tensile fracture stress of the hydrogels also increases in the same way and highest fracture stresses of 4–7 MPa could be obtained at f_{cry} above 10% (Fig. 4B). On the other hand, elongation at break decreases from ~400% to ~5% with increasing

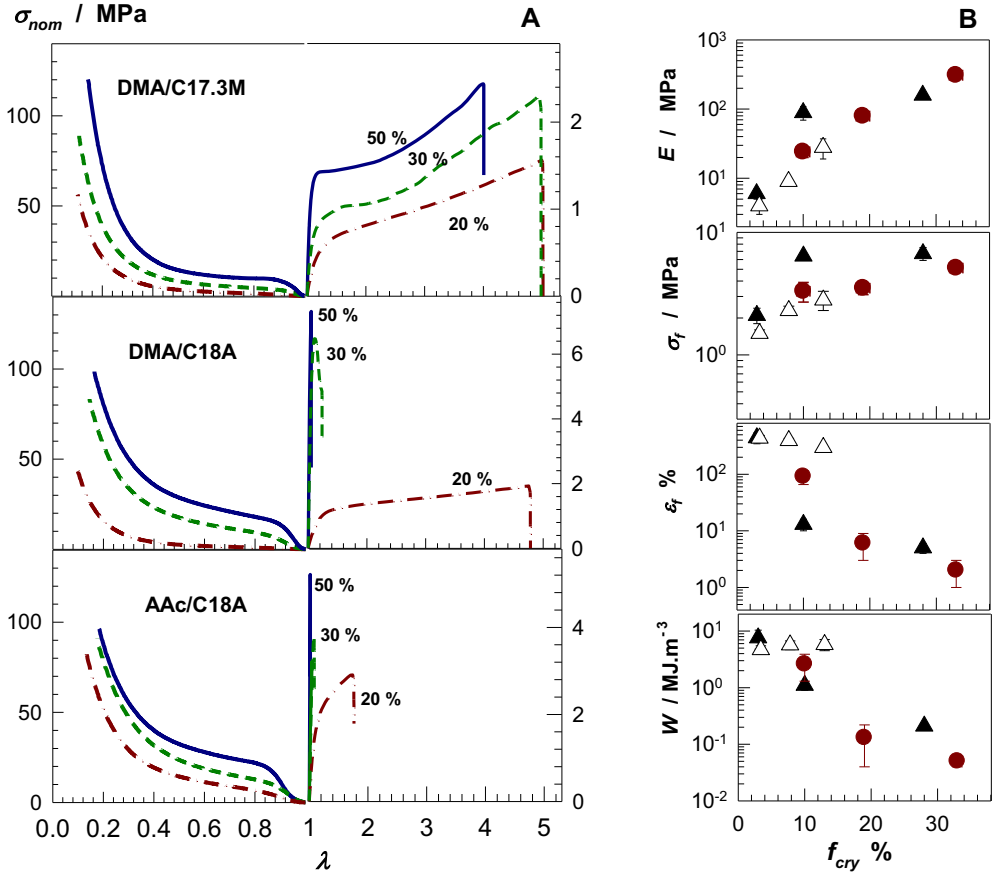

Fig. 4. (A) Stress σ_{nom} vs deformation ratio λ curves of the hydrogels from compression ($\lambda < 1$) and elongation tests ($\lambda > 1$). Hydrophobe content = 20 (dash-dot curves), 30 (dashed curves), and 50 mol% (solid curves). Strain rate ($\dot{\varepsilon}$) = 3.8×10^{-2} s^{-1}. (B) Young's modulus E, tensile fracture stress σ_f, fracture strain ε_f, and toughness W of the hydrogels plotted against the fraction f_{cry} of polymer units in crystalline domains. Strain rate ($\dot{\varepsilon}$) = 3.8×10^{-2} s^{-1}. Hydrogels: DMA/C17.3M (△), DMA/C18A (▲), AAc/C18A (●).

mechanical strength of the hydrogels. The results in Fig. 4A also show that the hydrogels with a degree of crystallinity f_{cry} - $\leqslant$ 13% exhibit yielding type behavior while those with f_{cry} between 19 and 33% fracture without yielding. This behavior was also observed in compression tests when the nominal compressive stress σ_{nom} is first converted to the true stress σ_{true} and σ_{true} is plotted against the deformation ratio (Fig. S1). The appearance of yielding type shape in stress-strain curves results in an increase in the elongation at break and energy to break (toughness) of the hydrogels. DMA/C17.3 hydrogels thus exhibit the highest toughness (5–6 MJ m^{-3}) and elongation at break (300–440%). We attribute the distinct yielding, and hence enhanced toughness and elongation at low f_{cry} to the internal rupture of crystalline domains by dissipating energy while at high f_{cry}, these domains are too strong to dissipate energy within the time scale of the mechanical tests ($\dot{\varepsilon} = 3.8 \times 10^{-2}$ s^{-1}).

We also measured the fracture energies G of the hydrogels by a single notch tear test [10,19]. The fracture energy G which is a measure of the resistance to crack propagation is in the range 3.6–20 kJ m^{-2} for $f_{cry} \leqslant 13\%$ (Table 1); these values are much larger than those reported before for stress-bearing hydrogels (Fig. 1). Mechanical testing thus demonstrates that the mechanical properties of the hydrogels could be tailored by varying the degree of crystallinity. For instance, DMA/C18A hydrogel at 20 mol% hydrophobe level (f_{cry} = 3%) contains ~47% water (Table 1), as the water content of cornea, cartilage, the dermis, and, arterial walls [3]. Its modulus E is about 6 MPa and tensile strength σ_f is about 2.1 MPa, which are comparable to those of cornea (σ_f = 4 MPa, E = 6 MPa) [3]. Moreover, the compressive modulus of the hydrogels with $f_{cry} \geqslant 8\%$ is between 40 and 190 MPa (Fig. S6), which are in the range of those of the natural lumbar intervertebral discs (IVDs) [43–45].

The mechanical data discussed above were obtained at a strain rate $\dot{\varepsilon}$ of 3.8×10^{-2} s^{-1}. Because of the physical nature of the crosslinks, the hydrogels exhibited strain rate sensitivity, i.e., increasing rate of strain also increased the modulus E, fracture stress σ_f, and the yield stress σ_y. This behavior is illustrated in Fig. 5A representing stress – strain curves of DMA/C18A hydrogel samples with 30 mol% hydrophobe at various strain rates $\dot{\varepsilon}$. By reducing the rate of strain from 7.8×10^{-2} to 4×10^{-3} s^{-1}, a brittle-to-ductile transition occurs with a 5–fold increase in toughness (from 1.1 to 5.2 MPa) and 7-fold increase in elongation to break (20–140%). In Fig. 5B, σ_y and E are plotted against the strain rate $\dot{\varepsilon}$. A linear relation between the yield strain σ_y and log ($\dot{\varepsilon}$) is seen from the figure, in accord with the prediction of the Eyring model of mechanically induced dissociation of molecular bonds as,

$$\dot{\varepsilon} \sim \exp\left(-\frac{E_a - \sigma V_a}{kT}\right) \tag{2}$$

where E_a is the activation energy, $\sigma = \sigma_y/2$ is the shear yield stress, V_a is the activation volume, k is the Boltzmann constant, and T is the absolute temperature [20,46,47]. The solid line in Fig. 5B showing the best fitting line yields $V_a = 11 \pm 1$ nm^3 and $E_a = 27 \pm 1$ kJ mol^{-1}. E_a is much smaller then covalent carbon-carbon bond energy (347 kJ mol^{-1}) while V_a is much larger than that reported for covalent systems [48,49]. This suggests activation of larger species like side alkyl chain crystals with a lesser amount of energy as compared to the covalently crosslinked polymer systems.

The existence of dynamic intermolecular bonds is also demonstrated by cyclic mechanical tests conducted at 23 ± 2 °C. The solid curves in Fig. 6A show compression cycles of hydrogel samples at a constant strain rate up to 90% compression, followed by immediate retraction to zero displacement. The loading curve of the compressive cycle is completely different from the unloading curve indicating damage in the gel samples and dissipation of energy during the cycle. After the first cycle, the gel remained in a compressed state, indicating complete energy loss after the cycle and thus, occurrence of an irreversible damage to the samples. However, when the compressed hydrogel samples are immersed in a water bath at 70 °C, the samples immediately recover their original dimensions so that they can be subjected to successive cycles. Dashed and

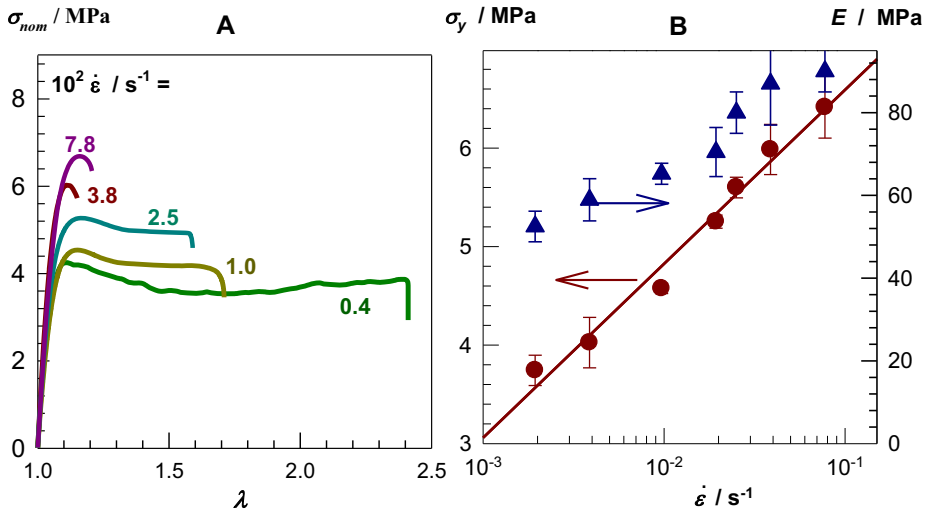

Fig. 5. (A) Stress σ_{nom} vs deformation ratio λ curves of DMA/C18A hydrogels with 30 mol% hydrophobe at various strain rates $\dot{\varepsilon}$. (B) Yield stress σ_y and the Young's modulus E plotted against the logarithm of the strain rate $\dot{\varepsilon}$. The solid line is the best fit to σ_y - log($\dot{\varepsilon}$) data.

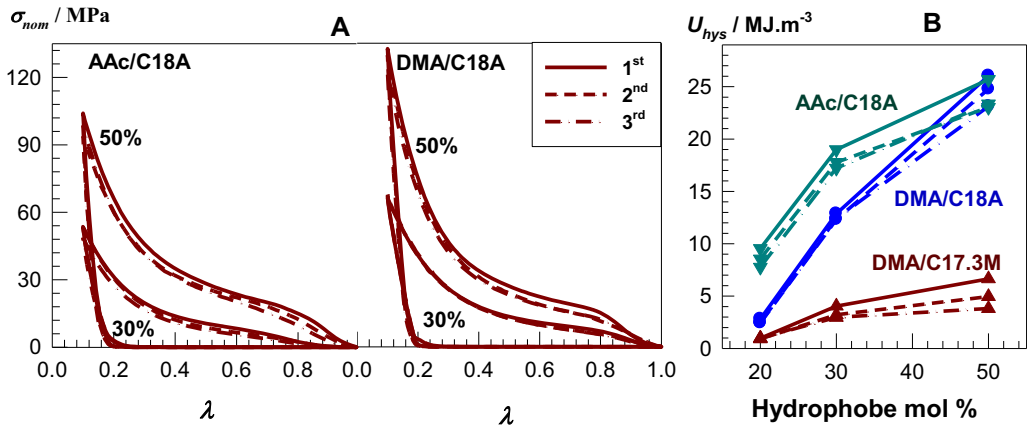

Fig. 6. (A) Three successive loading/unloading cycles up to 90% compression for the hydrogel samples indicated. Note that between each cycle, the gel samples were immersed in a water bath at 70 °C. (B) Hysteresis energies U_{hys} during the cyclic compression experiments shown as a function of the hydrophobe content of the hydrogels. 1st, 2nd, and 3rd cycles are presented by solid, dashed, and dash-dot curves, respectively.

dash-dot curves in Fig. 6A show 2nd and 3rd mechanical cycles of the gel samples conducted at 23 ± 2 °C after their immersion in water at 70 °C for 5 min. The good superposition of the successive loading curves demonstrates that the damage done to the hydrogel samples during the loading cycle is recoverable after heating above T_m of the crystalline domains. Similar results were also obtained by cyclic elongation tests (Fig. S7). The energy U_{hys} dissipated during the mechanical cycles was calculated from the area between the loading and unloading curves. Fig. 6B shows U_{hys} calculated from the compression cycles of the hydrogels plotted against their hydrophobe content. Increasing stability of the crystalline domains in the order of DMA/C17.3M < DMA/C18A < AAc/C18A also increases the hysteresis energy and it approaches to 25 MJ m^{-3} at 50 mol% C18A. This means that, although a large fraction of crystalline domains is destroyed under compression, heating the hydrogels above the melting temperature recovers the original microstructure.

Temperature induced recovery of the original mechanical properties of the hydrogels demonstrated in Fig. 6 reveals their abilities to self-heal and to memorize their permanent shape. Fig. 7A illustrates the self-healing and shape memory behavior

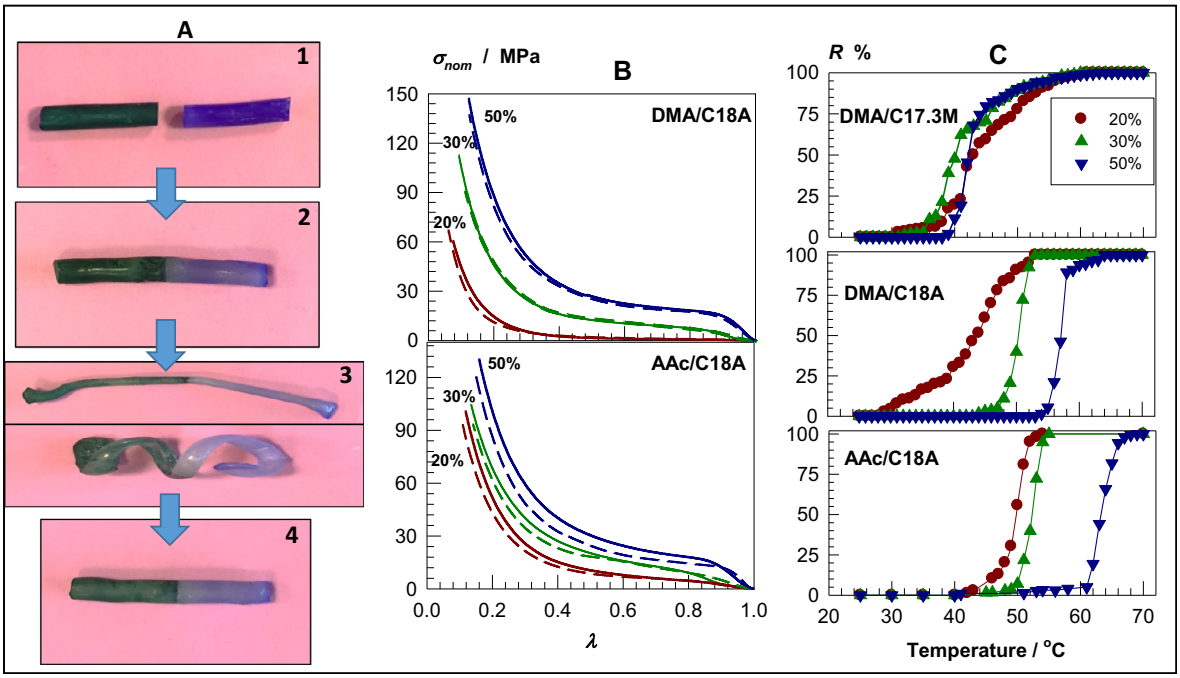

Fig. 7. (A) Photographs of two DMA/AAc hydrogel samples with 30 mol% hydrophobe showing its self-healing and shape-memory behavior. One of the gel samples is colored for clarity. After pressing the fractured surfaces together at 80 °C for 24 h, they merge into a single piece (2). When the healed gel sample is heated at 70 °C, any temporary shape can be given which can then be fixed by cooling to room temperature (3). On heating again to 70 °C, the gel sample recovers its original shape (4). (B) Stress-strain curves of virgin (solid curves) and healed gel samples (dashed curves). Hydrophobe contents are indicated. (C) Shape recovery ratio R of the hydrogels shown as a function of temperature. Hydrophobe contents are indicated.

of two DMA/AAc hydrogel samples with 30 mol% hydrophobe. After pressing the fractured surfaces of the samples together above T_m for 24 h, they merge into a single piece (2). After cooling, the healed gel sample exhibits its original mechanical properties (Fig. 7B). Moreover, when the healed gel sample is again heated above T_m, it becomes soft so that any temporary shape can be given which is then fixed by cooling the sample to 24 °C (3). By heating the gel sample in a water bath at 70 °C, it returns to its initial shape within 15 s (4).

To quantify the healing efficiency, compression testing experiments were performed using cylindrical gel samples of 5 mm in diameter and 6 cm in length. The samples were cut in the middle and then, the two halfs were merged together within a plastic syringe (of the same diameter as the gel sample) at 80 °C by slightly pressing the piston plunger. In Fig. 7B, stress-strain curves of the virgin (solid curves) and healed gel samples (dashed curves) are shown for a healing time of 24 h. The good superposition of the curves indicates a high healing efficiency for the hydrogels. The small differences observed in the stress-strain curves of virgin and healed AAc/C18A hydrogel samples may be attributed to a small extent of permanent damage in these highly crystalline hydrogels. For instance, healed DMA/C18A hydrogels with 50% hydrophobe sustain up to 138 ± 10 MPa stress under 87% compression, which is around 87% of the virgin gel samples. To determine the shape memory effect of the hydrogels, bending tests were utilized by recording the shape recovery ratio R at various temperatures. Fig. 7C shows the shape recovery ratio R of the hydrogels plotted against the temperature. All hydrogel samples exhibit shape-recovery ratios of 100% at or above 52 °C. For AAc/C18A hydrogels, the recovery ratio R equals to zero below 42 °C, indicating that the temporary shape remains unchanged, that is, the shape fixing efficiency is 100%. This reveals the ability of these gel samples to hold the temporary shape up to temperatures close to the transition temperature. For DMA/C17.3M hydrogels, the shape recovery ratio gradually increases with increasing temperature indicating that the crystalline domains in these hydrogels cannot support the residual stress in the network chains. This is consistent with the low degree of crystallinity of DMA/C17.3M hydrogels (Table 1). However, for the hydrogels with 30 and 50 mol% C18A, R increases from 0 to 100% over a rather small range of temperature. The results indicate that the hydrophobic units of the polymer chains act both as net-points and switching segments in the shape memory behavior of the hydrogels [50–53]. The hydrophobic units forming hydrophobic associations above T_m act as physical crosslinks, i.e., as netpoints to restore the random coil conformation of the deformed network chains. Below T_m, they form crystalline domains and thus acting as switching segments to fix the temporary shape.

4. Conclusions

We use hydrophobic interactions to generate a 3D network of PDMA and PAAc chains. Gelation under bulk conditions as well as formation of crystalline domains and hydrophobic associations between side alkyl chains generate high-strength hydrogels containing 7–56% water. In contrast to hybrid DN hydrogels consisting of chemically and physically crosslinked network components [12–14], our hydrogels consist of only physically crosslinked networks. The key to obtain high strength hydrogels is the co-existence of crystalline domains and hydrophobic associations acting as strong and weak physical cross-links, respectively. The appearance of yielding type shape in the stress-strain curves and a large irreversible hysteresis during the mechanical cycles indicate internal rupture of crystalline domains by dissipating energy. Thus, both types of crosslinks in our hydrogels contribute to the energy dissipation in the gel network and hence produce mechanically stronger hydrogels as compared to hybrid DNs.

The results show that both the transition temperatures and the degree of crystallinity increase with increasing hydrophobe level in the comonomer feed. C18A hydrophobe produces crystalline domains with a higher thermal stability as compared to C17.3M, which is attributed to the uniform length of its side alkyl chains as well as to the flexibility of acrylates backbones as compared to methacrylate ones. PAAc backbone produces a higher transition temperature and degree of crystallinity as compared to PDMA backbone due to the hydrogen bonding interactions between the carboxyl groups. The results reveal that the stability of crystalline domains in the hydrogels increases in the following order: DMA/C17.3M < DMA/C18A < AAc/C18A. By choosing suitable comonomer pairs and compositions, one may vary the degree of crystallinity f_{cry} between 3 and 33%, which leads to two orders of magnitude change in the modulus, elongation at break, and toughness. For instance, the modulus E increases with increasing f_{cry} and becomes 308 ± 16 MPa at f_{cry} = 33%, which is the highest modulus reported so far for high-strength hydrogels. Tensile fracture stress of the hydrogels also increases in the same way and highest fracture stresses of 4–7 MPa could be obtained at f_{cry} above 10%. The fracture energy G of the hydrogels is in the range 3.6–20 kJ m^{-2} for $f_{cry} \leqslant 13\%$; these values are much larger than those reported before for stress-bearing hydrogels. Mechanical testing thus demonstrates that the mechanical properties of the hydrogels could be tailored by varying the degree of crystallinity f_{cry}. The hydrogels exhibit self-healing and shape memory functions triggered by heating above the melting temperature of their crystalline domains. Healed hydrogels sustain up to 138 ± 10 MPa of compressive stress σ_f, which is around 87% of σ_f of the virgin samples.

Acknowledgments

This work was supported by the Scientific and Technical Research Council of Turkey (TUBITAK), KBAG 114Z312. OO thanks the Turkish Academy of Sciences (TUBA) for the partial support.

Appendix A. Supplementary material

Supplementary data associated with this article can be found, in the online version, at http://dx.doi.org/10.1016/j.eurpolymj.2016.05.019.

References

[1] S.J. Buwaldaa, K.W.M. Boerea, P.J. Dijkstrab, J. Feijenc, T. Vermondena, W.E. Henninka, Hydrogels in a historical perspective: from simple networks to smart materials, J. Control. Release 190 (2014) 254–273.
[2] E. Calo, V.V. Khutoryanskiy, Biomedical applications of hydrogels: a review of patents and commercial products, Eur. Polym. J. 65 (2015) 252–267.
[3] P. Calvert, Hydrogels for soft machines, Adv. Mater. 21 (2009) 743–756.
[4] M.F. Ashby, L.J. Gibson, U. Wegst, R. Olive, The mechanical properties of natural materials. I. Material property charts, Proc. R. Soc. Lond. A 450 (1995) 123–140.
[5] X. Zhao, Multi-scale multi-mechanism design of tough hydrogels: building dissipation into stretchy networks, Soft Matter 10 (2014) 672–687.
[6] Y. Tanaka, K. Fukao, Y. Miyamoto, Fracture energy of gels, Eur. J. Phys. E 3 (2000) 395–401.
[7] H.R. Brown, A model of the fracture of double network gels, Macromolecules 40 (2007) 3815–3818.
[8] A.M.S. Costa, J.F. Mano, Extremely strong and tough hydrogels as prospective candidates for tissue repair – a review, Eur. Polym. J. 72 (2015) 344–346.
[9] J.P. Gong, Y. Katsuyama, T. Kurokawa, Y. Osada, Double-network hydrogels with extremely high mechanical strength, Adv. Mater. 15 (2003) 1155–1158.
[10] Y. Tanaka, R. Kuwabara, Y.-H. Na, T. Kurokawa, J.P. Gong, Y. Osada, Determination of fracture energy of high strength double network hydrogels, J. Phys. Chem. B 109 (2005) 11559–11562.
[11] J.P. Gong, Why are double network hydrogels so tough?, Soft Matter 6 (2010) 2583–2590
[12] Q. Chen, D. Wei, H. Chen, L. Zhu, C. Jiao, G. Liu, L. Huang, J. Yang, L. Wang, J. Zheng, Simultaneous enhancement of stiffness and toughness in hybrid double-network hydrogels via the first, physically linked network, Macromolecules 48 (2015) 8003–8010.
[13] J. Li, Z. Suo, J.J. Vlassak, Stiff, strong, and tough hydrogels with good chemical stability, J. Mater. Chem. B 2 (2014) 6708–6713.
[14] J.-Y. Sun, X. Zhao, W.R.K. Illeperuma, O. Chaudhuri, K.H. Oh, D.J. Mooney, J.J. Vlassak, Z. Suo, Highly stretchable and tough hydrogels, Nature 489 (2012) 133–136.
[15] L. Zhang, J. Zhao, J. Zhu, C. He, H. Wang, Anisotropic tough poly(vinyl alcohol) hydrogels, Soft Matter 8 (2012) 10439–10447.
[16] K. Haraguchi, T. Takehisa, Nanocomposite hydrogels: a unique organic–inorganic network structure with extraordinary mechanical, optical, and swelling/de-swelling properties, Adv. Mater. 14 (2002) 1120–1124.
[17] K. Haraguchi, R. Farnworth, A. Ohbayashi, T. Takehisa, Macromolecules 36 (2003) 5732–5741.
[18] A. Klein, P.G. Whitten, K. Resch, G. Pinter, Nanocomposite hydrogels: fracture toughness and energy dissipation mechanisms, J. Polym. Sci., Part B: Polym. Phys. 53 (2015) 1763–1773.
[19] T.L. Sun, T. Kurokawa, S. Kuroda, A.B. Ihsan, T. Akasaki, K. Sato, M.A. Haque, T. Nakajima, J.P. Gong, Physical hydrogels composed of polyampholytes demonstrate high toughness and viscoelasticity, Nat. Mater. 12 (2013) 932–937.
[20] X. Hu, M. Vatankhah-Varnoosfaderani, J. Zhou, Q. Li, S.S. Sheiko, Weak hydrogen bonding enables hard, strong, tough, and elastic hydrogels, Adv. Mater. 27 (2015) 6899–6905.
[21] Q. Wang, J.L. Mynar, M. Yoshida, E. Lee, M. Lee, K. Okura, K. Kinbara, T. Aida, High-water-content mouldable hydrogels by mixing clay and a dendritic molecular binder, Nature 463 (2010) 339–343.
[22] N. Holten-Andersen, M.J. Harrington, H. Birkedal, B.P. Lee, P.B. Messersmith, K.Y.C. Lee, J.H. Waite, PH-induced metal–ligand cross-links inspired by mussel yield self-healing polymer networks with near-covalent elastic moduli, PNAS 108 (2011) 2651–2655.
[23] F. Liu, F. Li, G. Deng, Y. Chen, B. Zhang, J. Zhang, C.-Y. Liu, Rheological images of dynamic covalent polymer networks and mechanisms behind mechanical and self-healing properties, Macromolecules 45 (2012) 1636–1645.
[24] S.B. Quint, C. Pacholski, Extraordinary long range order in self-healing non-close packed 2D arrays, Soft Matter 7 (2011) 3735–3738.
[25] A. Phadke, C. Zhang, B. Arman, C.-C. Hsu, A. Mashelkar, A.K. Lele, M.J. Tauber, G. Arya, S. Varghese, Rapid self-healing hydrogels, PNAS 109 (2012) 4383–4388.
[26] O. Okay, Self-healing hydrogels formed via hydrophobic interactions, Adv. Polym. Sci. 268 (2015) 101–142.
[27] U. Gulyuz, O. Okay, Self-healing poly(N-isopropylacrylamide) hydrogels, Eur. Polym. J. 72 (2015) 12–22.
[28] F. Ding, S. Wu, S. Wang, X. Xiong, Y. Li, B. Li, H. Deng, Y. Du, L. Xiao, X. Shi, A dynamic and self-crosslinked polysaccharide hydrogel with autonomous self-healing ability, Soft Matter 11 (2015) 3971–3976.
[29] S. Mukherjee, M.R. Hill, B.S. Sumerlin, Self-healing hydrogels containing reversible oxime crosslinks, Soft Matter 11 (2015) 6152–6161.
[30] T. Kakuta, Y. Takashima, M. Nakahata, M. Otsubo, H. Yamaguchi, A. Harada, Preorganized hydrogel: self-healing properties of supramolecular hydrogels formed by polymerization of host–guest-monomers that contain cyclodextrins and hydrophobic guest groups, Adv. Mater. 25 (2013) 2849–2853.
[31] U. Gulyuz, O. Okay, Self-healing poly(acrylic acid) hydrogels with shape memory behavior of high mechanical strength, Macromolecules 47 (2014) 6889–6899.
[32] H. Meng, P. Xiao, J. Gu, X. Wen, J. Xu, C. Zhao, J. Zhang, T. Chen, Self-healable macro-/microscopic shape memory hydrogels based on supramolecular interactions, Chem. Commun. 50 (2014) 12277–12280.
[33] H. Zhang, D. Han, Q. Yan, D. Fortin, H. Xia, Y. Zhao, Light-healable hard hydrogels through photothermally induced melting–crystallization phase transition, J. Mater. Chem. A 2 (2014) 13373–13379.
[34] Z. Mogri, D.R. Paul, Gas sorption and transport in side-chain crystalline and molten poly(octadecyl acrylate), Polymer 42 (2001) 2531–2542.
[35] H.S. Bisht, P.P. Pande, A.K. Chatterjee, Docosyl acrylate modified polyacrylic acid: synthesis and crystallinity, Eur. Polym. J. 38 (2002) 2355–2358.
[36] M.G. Broadhurst, An analysis of the solid phase behavior of the normal paraffins, J. Res. Natl. Bur. Stand. A 66A (1962) 241–249.
[37] E.F. Jordan, D.W. Feldeisen, A.N. Wrigley, Side-chain crystallinity. I. Heats of fusion and melting transitions on selected homopolymers having long side chains, J. Polym. Sci. A-1: Polym. Chem. 9 (1971) 1835–1851.
[38] C. Bilici, O. Okay, Shape memory hydrogels via micellar copolymerization of acrylic acid and *n*-octadecyl acrylate in aqueous media, Macromolecules 46 (2013) 3125–3131.
[39] T. Miyazaki, K. Yamaoka, J.P. Gong, Y. Osada, Hydrogels with crystalline or liquid crystalline structure, Macromol. Rapid Commun. 23 (2002) 447–455.
[40] S. Abdurrahmanoglu, V. Can, O. Okay, Design of high-toughness polyacrylamide hydrogels by hydrophobic modification, Polymer 50 (2009) 5449–5455.
[41] L.R.G. Treloar, The Physics of Rubber Elasticity, University Press, Oxford, 1975.
[42] P.J. Flory, Principles of Polymer Chemistry, Cornell University Press, Ithaca, NY, 1953.
[43] A. Gloria, F. Causa, R.D. Santis, P.A. Netti, L. Ambrosio, Dynamic-mechanical properties of a novel composite intervertebral disc prosthesis, J. Mater. Sci. – Mater. Med. 18 (2007) 2159–2165.
[44] B.H. Wang, G. Campbell, Formulations of polyvinyl alcohol cryogel that mimic the biomechanical properties of soft tissues in the natural lumbar intervertebral disc, Spine 34 (2009) 2745–2753.
[45] N.L. Nerurkar, D.M. Elliott, R.L. Mauck, Mechanical design criteria for intervertebral disc tissue engineering, J. Biomech. 43 (2010) 1017–1030.
[46] W. Kauzmann, H. Eyring, The viscous flow of large molecules, J. Am. Chem. Soc. 62 (1940) 3113–3125.

[47] N.G. McCrum, C.P. Buckley, C.B. Bucknall, Principles of Polymer Engineering, Oxford University Press, New York, 1997.
[48] M.F. Omar, H.M. Akil, Z.A. Ahmad, Particle size – dependent on the static and dynamic compression properties of polypropylene/silica composites, Mater. Des. 45 (2013) 539–547.
[49] L. Vanel, S. Ciliberto, P.-P. Cortet, S. Santucci, Time-dependent rupture and slow crack growth: elastic and viscoplastic dynamics, J. Phys. D Appl. Phys. 42 (2009) 214007.
[50] A. Lendlein, S. Kelch, Shape-memory polymers, Angew. Chem. – Int. Ed. 41 (2002) 2034–2057.
[51] C. Liu, H. Quin, P.T. Mather, Review of progress in shape-memory polymers, J. Mater. Chem. 17 (2007) 1543–1558.
[52] M. Behl, A. Lendlein, Actively moving polymers, Soft Matter 3 (2007) 58–67.
[53] M. Behl, Y. Razzaq, A. Lendlein, Multifunctional shape-memory polymers, Adv. Mater. 22 (2010) 3388–3410.